ISSN: 2148-9173 **Vol: 8 Issue:3 September 2021**

International Journal of Environment and Geoinformatics (IJEGEO) is an international, multidisciplinary, peer reviewed, open access journal.

Investigating Time Dependent Stress Changes Globally Following Large Earthquakes (M≥7)

Fatih SUNBUL

Abstracting and Indexing: TR DIZIN, DOAJ, Index Copernicus, OAJI, Scientific Indexing Services, International Scientific Indexing, Journal Factor, Google Scholar, Ulrich's Periodicals Directory, WorldCat, DRJI, ResearchBib, SOBIAD

International Journal of Environment and Geoinformatics 8(3):376-385 (2021)

Reaserch Article

Investigating Time Dependent Stress Changes Globally Following Large Earthquakes (M≥7)

Fatih Sünbül

İzmir Bakırçay University, Faculty of Science and Arts, Department of Geography, İzmir, TR

E-mail: fatih.sunbul@bakircay.edu.tr

Received 09.01.2021
Accepted 12.04.2021

How to cite: Sünbül (2021). Investigating Time Dependent Stress Changes Globally Following Large Earthquakes (M≥7), *International Journal of Environment and Geoinformatics (IJEGEO)*, 8(3):376-385. doi. 10.30897/ijegeo. 857112

Abstract

Triggered earthquakes can cause disproportionate damages depend on their magnitudes. In fact, there is a causal link between the spatial distribution of those events and the stress changes induced by the mainshock. Co-seismic stress loading is one of the key factors in determination of triggering mechanism. However, the time lags ranging hours to years and the stress diffusion over wider areas cannot be evaluated with the co-seismic process alone. In some cases, the stress interactions for long periods and larger areas can be attributed to post-seismic viscoelastic relaxations. In this study, M≥7 earthquakes from the Global Centroid Moment Tensor (GMCT) catalogue are modelled as dislocations to calculate shear stress changes on following earthquake nodal planes near enough to be triggered. The catalogue scanned for all other events (4.5<M<7) that occurred within ±2° from the centroid rupture planes. According to Omori law, which is one of the most reliable time predictable diagram of aftershock distributions, 10-year periods were used for the stress calculations. The events that had computed within ±0.01 to ±1 MPa stress change limits, considered as potential triggered events. The global co-seismic stress calculations show that 60.6% of the triggered events occurred in regions where the shear stress increased. The global stress change by incorporation viscous flow into co-seismic stress change were also tested. In this case, an increase in the rate of triggered events in both positive (15%) and negative (9%) shear stress areas were obtained. Despite the rate of triggered events has climbed significantly in both areas, only 2% of the changes have been computed globally. These rates are highly depending on fault mechanism across the plate boundaries. Thrust faults in the catalogue, for example, influence the stress distribution over broader regions and the dimension of fault ruptures. Therefore, thrust faults in the catalogue prevails the global statistics for both co-seismic and viscoelastic stress calculations. The results also demonstrate the significant effect of viscous flow, following large earthquakes, which cannot be neglected in stress interaction analysis.

Keywords: Global CMT Catalogue, Coulomb Stress, Viscoelastic Relaxation, Omori Law

Introduction

Based on geodetic measurements of deformations, the seismic cycle is divided into three main phases, which, taken separately or together, are the focus of all earthquake stress interaction studies. These phases are as follows: (a) the inter-seismic period; (b) the co-seismic period; and (c) the post-seismic period (Scholz, 2019). In all seismic periods in a cycle, two physical parameters should be defined. These are the *state of stress* and *its variation in time*, and together they control the earthquake phenomena. When an earthquake occurs on a fault plane it causes an increase or decrease in stress on neighboring faults. This 'retards' or 'hastens' the development of seismic events. The causal link between 'stress changes' and 'earthquake triggering' has significant implications for earthquake hazard analysis. Identifying areas of heightened or depressed seismic hazard enables us to understand the ways in which faults can influence the stress state of neighboring faults in the future (Harris, 1998; Steacy, 2005). The studies have shown that large earthquakes induce three types of deformation at least, visco-and poro-elastic relaxations and frictional afterslip (Taylor, 1996; Pollitz, 2003; Lemenkova., 2019).

The seismic hazard represented by a fault, averaged over numerous seismic cycles (10^2-10^4 yrs), is controlled primarily by the fault slip-rate because earthquake recurrence interval for a given magnitude of damaging earthquake on a specific fault, are shorter for higher slip rates (Stein, 2003). However, depending on the geometry of the faults, the seismic hazard represented by stress changes, with following rupture on the neighbouring faults either brought forward in time or delayed (McCloskey et al., 2005). A key element in the stress calculation is the knowledge of the elapsed time since the last damaging earthquake, as the stress renewal process, whereby faults are re-loaded either by regional stress or viscoelastic stress (Sunbul et al., 2016). Among those unknowns, one approach to the problem is determining to what extent an earthquake may influence successive events by utilizing static Coulomb stress calculations (King et al., 1994; McCloskey et al., 2003). Earthquakes cause stress perturbation in the neighbouring seismogenic zones of the fault rupture and an alteration in seismicity rate which demonstrates a possible causal link between seismicity rate and seismic hazard analysis (Steacy, 2005). In some cases, this triggering mechanism may

explain the seismic activity in the near regions which result in induced or retard seismic activity after a large earthquake (Nalbant et al., 1998; Stein et al., 1997). The earliest evidence to highlight the pattern of triggered events was the 1906 San Francisco, California earthquake (Parsons, 2002a). The stress analysis of the earthquake shows a decrease in total stress which leads to seismicity rate suppression along the fault zone (Toda et al., 2012). On the other hand, a sequence of several earthquakes occurred in Eastern California Shear Zone (ECSZ) that shows a causal link between the stress build up and increased triggering mechanism across the region. The 1990 M_w = 6.1 Joshua Tree event was supposedly triggered by the 1992 M_w = 7.3 Landers event where the 1999 M_w = 7.1 Hector Mine was the subsequent event in the sequence (Freed et al., 2007). Freed and Lin (2002), for example, calculated both co-seismic and post-seismic stress transfer on the 1999 Hector Mine fault due to the 1992 Landers earthquake and hypothesized that the Hector Mine rupture initiated at a location where co-seismic Coulomb stress increases were insufficient to induce failure, but post-seismic lower crustal stress transfer increase was sufficient to bring the fault to failure, thus explaining the delayed triggering of the Hector Mine event. Analysis of stress interactions include an assumption if an earthquake occurs in an elastic medium. In fact, following a large earthquake, stress diffuses within elastic crust and viscoelastic upper mantle, which result in producing viscoelastic deformations up to decades (Pollitz, 2003; Vergnolle et al., 2003).

Aftershocks or triggered events are characterized having lower magnitude that are distributed over the fault rupture, following a larger earthquake. According to the Omori's law (Omori, 1902) the number of aftershocks decays with the reciprocal of time "t^{-1}" following the main shock. Utsu, (1962) provided a slightly better match by implementing c/(p+n) where c, p and n are constants varying from one to the other in each earthquake series. This exponential decay, which shows the process of declining a number of events by a consistent percentage rate over a time period, is one of the few accurately time-predictable diagram of seismic hazard in a given area (Parsons, 2002b).

Limited publications regarding the rate of triggered earthquakes outside the classical aftershock zone demonstrate that the clusters illustrate the same temporal decay as aftershocks. Hence the process of stress transfer might apply to all earthquake catalogue data. Parsons (2002b) used this idea for the first time ignoring the post-seismic deformations in his model. The study brings new insights into global stress studies by incorporation of VE flow model in calculations. Here, I calculate co-seismic and visco-elastic deformations globally to evaluate how much the VE flow is effective on triggering mechanisms.

Materials and Methods

The Null Hypothesis

Limited study of the rate of triggered earthquakes outside the classical aftershock zone shows clusters that exhibit the same temporal decay as aftershocks, implying that the process of stress transfer may apply to all the events (i.e. Malmann and Parsons, 2008). I utilize global CMT catalogue to determine the triggering mechanisms on M<7 earthquakes following large events (M≥7) during co-seismic and post-seismic periods. I followed 3 main steps to calculate the global stress interactions between events.

a) All M≥7 earthquakes (109 events) were selected as candidates for evaluating the triggering in the CMT catalogue within 1990-2000 time-period (Fig. 1). Each fault plane solutions (strike, dip and rake angle) of the candidate events obtained from the CMT inversions were implemented as elastic rectangular dislocations from Wells and Coppersmith, (1994). In order to evaluate general observations on the orientation and distribution of average focal mechanisms of the main shocks, Frohlich (1992) statistical approach was used. Pure focal mechanisms depend on which principal stress axis (P, T and B-axes) is vertical; thrust when the T-axis is vertical; strike-slip when the B-axis is vertical, and normal when the P-axis is vertical. Following the Frohlich (1992) approach, focal mechanisms as thrust when the plunge of the P axis is greater than 50º, and normal or strike slip when the plunge of the T or B axis is greater than 60º were classified, respectively. The error range on the focal mechanisms in the CMT Catalogue is defined as between 0 to 15º (Frohlich, 2001). The average focal mechanisms of mainshocks were demonstrated in Appendices.

b) There is a causal link between the spatial distribution of aftershocks (receiver faults) and the stress changes caused by mainshock within a predictable distance and time. In order to identify those potentially triggered events from the catalogue, I select all lower magnitude events (4.5<M<7) that clustered within a 240 km radius ellipse, for 10 years (Fig. 2). Nodal planes of these earthquakes were represented as nonsliping dislocations, or receiver faults.

c) Instead of direct calculation of Coulomb stress, I modelled shear stress changes on each potentially triggered event (receiver faults). This is because, changes in shear stress are equivalent on both nodal planes of receiver faults, and there is no need to get any information of the friction of coefficient and pore pressure usually depend on local geologic structure. Although local parameters are known in well-studied areas such as California San Andreas or North Anatolian Fault Zones (Gazioğlu et al., 2002, 2005; Hébert et al., 2005), it is almost impossible to estimate or model local parameters in such global studies. Furthermore, the events that had computed shear stress changes between the limits of ±0.01 to ±1 MPa were considered as potential triggered events. The same limit was also used in previous studies to avoid unknown effects of coarse slip distributions in stress calculations very close to the rupture planes (i.e. Harris 1998; Parsons, 2002).

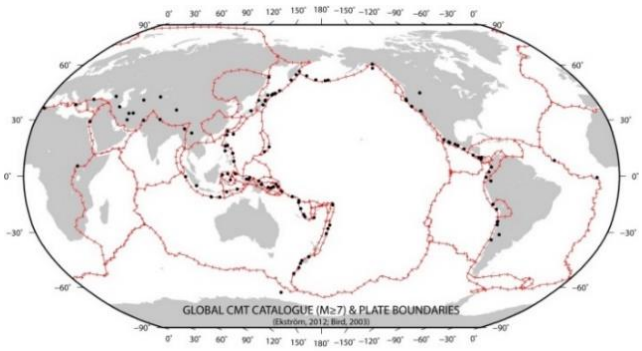

Fig. 1. Plate boundary map (Bird, 2009) shows M≥7 modelled earthquakes from Global CMT Catalogue (Ekström et al., 2012).

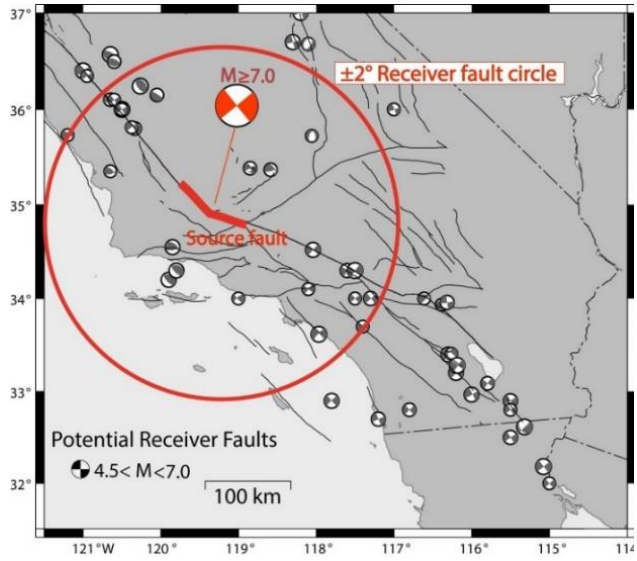

Fig. 2. Selection criteria for potential aftershocks. Shear stress changes were computed on each receiver faults/potentially triggered events (strike, dip and rake angle) obtained from the CMT Catalogue.

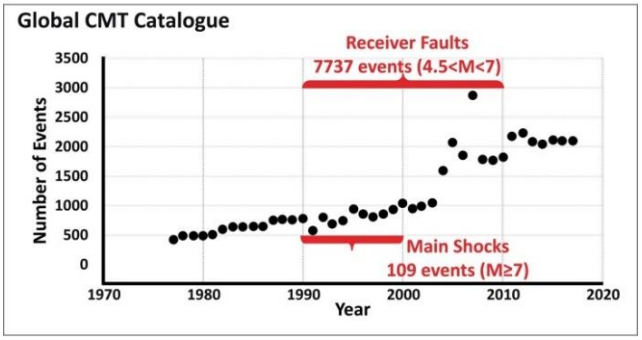

Fig. 3. The number of mainshocks and triggered events (receiver faults) given in a time frame. All candidate events were selected on continuous CMT Catalogue. Of these 109 events modelled as dislocations and all stress changes were computed on aftershocks within a 240 km radius ellipse in 10-year period after each main shock.

Co-Seismic Stress Calculations

In order to express stress changes in fault segments, a Coulomb stress criterion is used;

$$\Delta\sigma f = |\Delta\tau| + \mu'\Delta\sigma n + \Delta\rho \qquad (1)$$

where $|\Delta\tau|$ is the shear stress change, $\Delta\sigma n$ is the normal stress on the receiver fault plane orientation, $\mu'$is the apparent coefficient of friction and $\Delta\rho$ is pore pressure variation (Freed, 2005; King, 2007). All stress change calculations were resolved on dislocations planes; no point calculations were used (Okada, 1992). The strike, dip and rake of the 109 M≥7 earthquakes were used to create the elastic dislocation models. Dislocation length, width and slip were determined from global regressions of Wells and Coppersmith (1994).

Viscoelastic Stress Calculations

In terms of long term stress analysis (up to decades), viscoelastic relaxation mechanism can better illustrates stress triggering mechanism over long time periods and large distances (Freed, 2005). Stress relaxation response within a time dependent process $\sigma(t)$ (steady strain) and time dependent creep relaxation response $\varepsilon(t)$ (steady stress) are the components of any linear visco-elastic (VE) system (Wright et al., 2013). The Maxwell linear VE material is the most broadly used rheology model in crustal deformation analysis (Freed and Lin, 1998; Hearn et al., 2002; Johnson and Segall, 2004). Researchers have also proposed that the inelastic lithosphere ought to be modelled with a bi-viscous rheology, using a Burgers rheology (Pollitz, 2003). I use Burgers rheology model which includes Maxwell fluid and Kelvin solid components (Fig 3).

The Maxwell rheology involves an elastic component with shear modulus (μ) and a viscous component with viscosity (η), duration of relaxation is defined by (τ_M). Maxwell rheology is defined by;

$$\tau_M = \frac{\eta}{\mu} \qquad (2)$$

The Kelvin rheology (elastic and viscous components aligned parallel) has shear moduli μ_k and μ_e respectively where viscous components defined as η. Relaxation times τ_K and τ_S are expressed as

$$\tau_K = \eta / \mu_k \qquad (3)$$

and

$$\tau_S = \eta/ (\mu_k + \mu_e) \qquad (4)$$

Shear modulus (μ`) can be defined in a standard linear solid element is:

$$\mu` = \frac{\mu k\, \mu e}{(\mu k + \mu e)} \qquad (5)$$

Equation (5) corresponds to long term shear strength of a medium (Pollitz, 1997).

1D spherically stratified earth in the software (Fortran subroutines) designed by (Pollitz, 1997) was used during the calculations. The earth stratification model consists of both elastic and viscoelastic medium (Fig 4). The numerical analysis calculates the deformations in toroidal and spheroidal components in a spherical half space. Earth stratification model is illustrated with a Burgers

body rheology in the asthenosphere and Maxwell rheology in upper and lower mantle. Rheology values are $\eta_1 = 10^{19}$ Pa s, $\eta_2 = 5 \times 10^{17}$ Pa s, $\eta_{UM} = 10^{20}$ Pa s, $\eta_{LM} = 10^{21}$ Pa s., respectively. The time dependent relaxations have been calculated within the time period of each main shock' initiation till occurrence time of the triggered event. Those deformations, then, were converted to shear stress values.

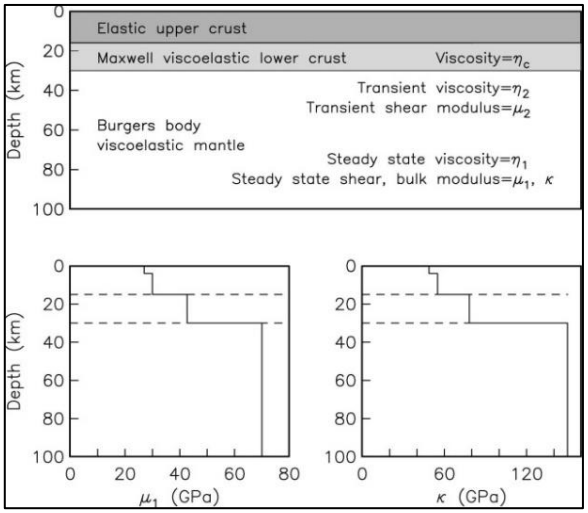

Fig. 4. Earth stratification model used in VE stress calculations (Pollitz, 2003).

Results

Co-seismic Stress Changes

A total of the 2626 events following the mainshocks that met the stress threshold selection criteria (±0.01 to ±1 MPa); of these 1592 events were associated by shear stress increases, and the remaining 1034 events associated by shear stress decreases (Fig. 5). Spotting at the shear stress component of the stress tensor in as a percentage, I find globally that 60.6% of the earthquakes occurred in regions where there was an increase in shear stress. All results have been also displayed in a separate document in APENDICES Table A1.

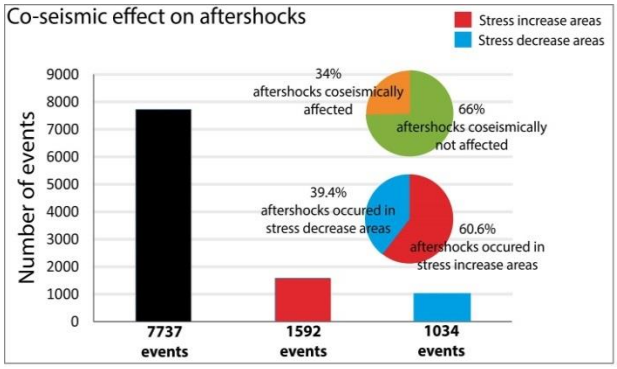

Fig. 5. Co-seismic stress change percentage on receiver faults.

Co-seismic Stresses Combined with VE Stress Change

Co-seismic stress calculation has been also combined with post-seismic VE stress change. Incorporating time dependent VE relaxations (CO+VE) into total shear stress calculations, I observe a significant increase in the number of potential triggered events in both positive and negative areas. Despite the number of triggered events have increased in both cases, there is only~2% change obtained in a global rate (Fig. 6).

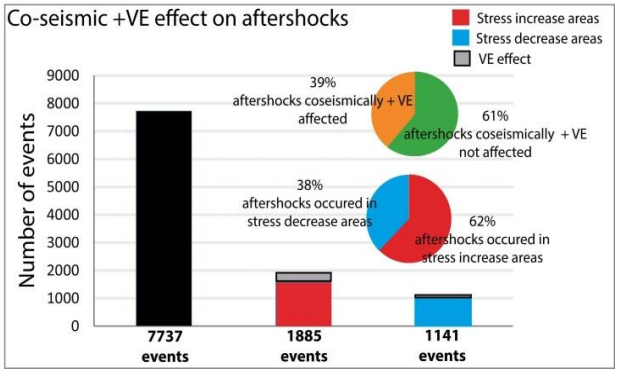

Fig. 6. Co-seismic stress change combined with viscoelastic deformations on receiver faults.

Average Fault Mechanisms of Mainshocks

Following the Frohlich (1992) approach, focal mechanisms as thrust when the plunge of the P axis is greater than 50º, and normal or strike slip when the plunge of the T or B axis is greater than 60º were classified. CMT catalogue which covers the 1990-2000 timespan imply that earthquakes occur more frequently on reverse faults (82%) than on strike slip (9%) and normal faults (5%). I also obtain of 4% of oblique faults, somehow ambiguous slip characteristics in focal mechanism solutions (Fig. 7).

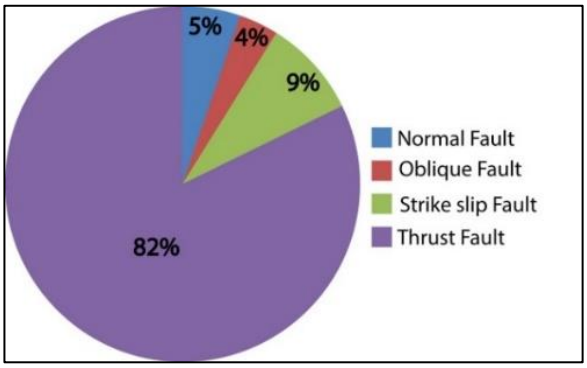

Fig. 7. Percentage distribution of main shocks due to their average fault mechanisms.

In comparison with different mechanisms in the co-seismic stress analysis; in the strike-slip and normal faulting, the aftershock rate occurring in the positive stress regions was lower than the aftershock rate occurring in the negative stress regions whereas this is the opposite in thrust and oblique faults. In thrust faults, the rate of aftershocks in the positive area is 63%, while the rate in the negative areas is 37%. In oblique faults, the rate of aftershocks within positive areas is 62%, and the rate for negative area is 38%. In normal faults, the aftershock rate in the negative area is 54%, while the aftershock rate in the positive area is 46%. In the strike-slip faults, the aftershock rate in the negative area was 59%, while the aftershock rate in the positive area was 41% (Fig. 8).

In comparison with various mechanisms incorporating viscous flow into the co-seismic stress analysis; in the strike-slip and normal faulting, the aftershock rate occurring in the positive stress regions was lower than the aftershock rate occurring in the negative stress regions whereas this is the opposite in thrust and oblique faults. In thrust faults, the rate of aftershocks in the positive area is 65%, while the rate in the negative areas is 35%. In oblique faulting, the rate of aftershocks within positive areas is 58%, and the rate for negative area is 42%. In normal faults, the aftershock rate in the negative area is 55%, while the aftershock rate in the positive area is 45%. In the strike-slip faulting, the aftershock rate in the negative area was 58%, while the aftershock rate in the positive area was 42% (Fig. 9).

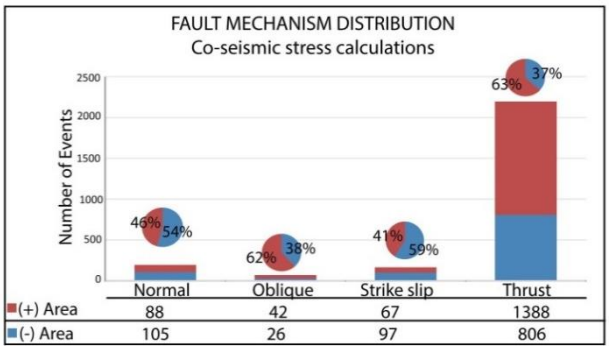

Fig. 8. Co-seismic stress distribution over various fault mechanism from the catalogue.

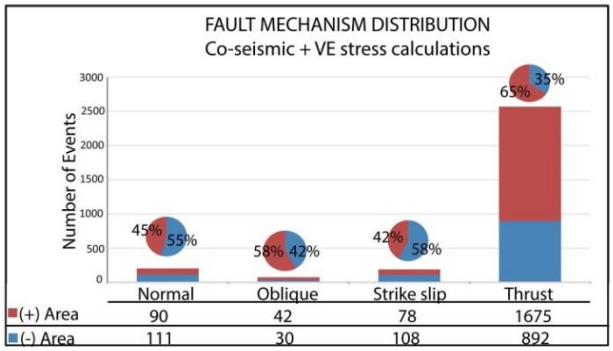

Fig. 9. Co-seismic plus viscoelastic stress distribution over various fault mechanism from the catalogue.

Discussion and Conclusion

Since there have been few systematic reviews on investigating of VE stress change on global triggering mechanism, 109 main earthquakes (M≥7) from Global CMT Catalogue with well-defined nodal planes and 7737 potentially triggered events (4.5<M<7) were modelled in the calculations. The analysis indicates that, the 2626 events could have been influenced by the source main events in the CMT catalogue; 1885 (60.6%) of them are related with computed co-seismic shear stress increase, while 1034 (39.4%) are related with shear stress decrease. Incorporation of VE effect into stress calculations, I obtain an increase in the rate of triggered events in both positive (15%) and negative (9%) shear stress areas. Despite increasing the rate of triggered events significantly in both areas, the global change remained relatively stable, has changed approximately 2%.

Stress rate variations have been observed in various fault mechanisms (Parsons et al., 1999). The focal mechanism of the large earthquakes (M≥7) alters stress state therefore the rate and of aftershocks can be modified. Across the subduction zones, thrust faulting mechanism shifts the entire elastic crust and results in modification of stress variation over broad regions (Dmowska et al., 1988; Taylor et al., 1996; 1998). Recent studies show that highest number of the potential aftershocks occur in stress increase off fault lobes following large earthquakes (Freed, 2005). One study reports that strike slip mechanism faulting only change smaller section of the fault plane (Parsons et al., 1999). The results in the study were quite compatible with the previous research; the number of triggered earthquakes in the catalogue has been seismically prevailed by subduction zone source events.

Large events influence the stress distribution over broader regions and the dimension of fault rupture associates with stress distribution size. Casarotti et al., (2001) investigated the stress interactions of 8 large earthquakes in Pacific zone. Their results show that large earthquakes modify the seismicity along the boundaries and most triggered events occurs across the plate boundaries. The results here also show a similar conclusion, I got more triggered events clustered across the large event fault rupture zones.

Viscoelastic relaxations can cause stress distribution over a wider area and during long time period up to decades (Chéry et al., 2001). Due to viscoelastic relaxations; strike slip faults, for example, stress increase areas in Coulomb stress change calculations tend to increase in magnitude and stress decrease areas tend to decrease in magnitude as well. However, this process being adversely in thrust faulting mechanism. Due to relaxation process, stress increase areas tend to decrease in magnitude, stress decrease areas vice versa (Freed and Lin, 1998; Lin and Stein, 2004; Nostro et al., 2001). The results in this study are in good agreement with previous reports that the number of aftershocks is significantly raised by up to 17% when incorporation of VE flow in stress modelling. Global analysis shows that the viscoelastic relaxation has a significant influence on the deformations following large earthquakes, which should not be eliminated in stress interactions.

References

Bird, P. (2009). Long-term fault slip rates, distributed deformation rates, and forecast of seismicity in the western United States from joint fitting of community geologic, geodetic, and stress direction data sets. Journal of Geophysical Research: Solid Earth, *114*(B11). doi.org/10.1029/2009JB006317.

Casarotti, E., Piersanti, A., Lucente, F., Boschi, E. (2001). Global postseismic stress diffusion and fault interaction at long distances. *Earth and Planetary Science Letters*, *191*(1–2), 75–84.doi.org/ 10.1016/S0012-821X(01)00404-6

Chéry, J., Carretier, S., Ritz, J.-F. (2001). Postseismic stress transfer explains time clustering of large earthquakes in Mongolia. *Earth and Planetary Science*

Letters, *194*(1–2), 277–286. doi.org/10.1016/S0012-821X(01)00552-0.

Dmowska, R., Rice, J. R., Lovison, L. C., Josell, D. (1988). Stress transfer and seismic phenomena in coupled subduction zones during the earthquake cycle. *Journal of Geophysical Research*, *93*(B7), 7869. doi.org/10.1029/JB093iB07p07869

Ekström, G., Nettles, M., Dziewoński, A. M. (2012). The global CMT project 2004–2010: Centroid-moment tensors for 13,017 earthquakes. *Physics of the Earth and Planetary Interiors*, *200–201*, 1–9. doi.org/10.1016/j.pepi.2012.04.002

Freed, A. M. (2005). Earthquake Triggering by Static, Dynamic, and Postseismic Stress Transfer. *Annual Review of Earth and Planetary Sciences*, *33*(1), 335–367. doi.org/10.1146/annurev.earth.33.092203.122505

Freed, A. M., Ali, S. T., Bürgmann, R. (2007). Evolution of stress in Southern California for the past 200 years from co-seismic, postseismic and interseismic stress changes. *Geophysical Journal International*, *169*(3), 1164–1179. doi.org/10.1111/j.1365-246X.2007.03391.x

Freed, A. M., Lin, J. (1998). Time-dependent changes in failure stress following thrust earthquakes. *Journal of Geophysical Research: Solid Earth*, *103*(B10), 24393–24409. doi.org/10.1029/98JB01764

Gazioglu C, Gokasan E, Algan O, Yucel ZY, Tok B., Dogan E (2002) Morphologic features of the Sea of Marmara from multibeam data. Marine Geology, 190:397–420.

Gazioğlu C, Yucel ZY., Dogan E (2005) Morphological features of major submarine landslides of Sea of Marmara using multibeam data. J Coastal Research, Vo. 21:664–673.

Harris, R. A. (1998). Introduction to Special Section: Stress Triggers, Stress Shadows, and Implications for Seismic Hazard. *Journal of Geophysical Research: Solid Earth*, *103*(B10), 24347–24358. doi.org/10.1029/98JB01576

Hearn, Elizabeth H. (2002). Viscoelastic Deformation from North Anatolian Fault Zone Earthquakes and the Eastern Mediterranean GPS Velocity Field. *Geophysical Research Letters* 29(11):1549. doi: 10.1029/2002GL014889.

Hébert, H., Schindele, F., Altinok, Y., Alpar, B., Gazioglu, C. (2005). Tsunami hazard in the Marmara Sea (Turkey): a numerical approach to discuss active faulting and impact on the Istanbul coastal areas. *Marine Geology,* 215(1-2), 23-43.

Johnson, K. M., P. Segall (2004). Viscoelastic earthquake cycle models with deep stress-driven creep along the San Andreas fault system, J. Geophys. Res., 109, B10403, doi:10.1029/2004JB003096.

King, G.C.P. (2007). Fault Interaction, Earthquake Stress Changes, and the Evolution of Seismicity. In *Treatise on Geophysics* (pp. 225–255). doi.org/10.1016/B978-044452748-6.00069-9

King, G.C.P., Stein, R. S., Lin, J. (1994). Static stress changes and the triggering of earthquakes. *Bulletin of the Seismological Society of America*, *84*(3), 935–953.

Lemenkova, P. (2019). Generic Mapping Tools and Matplotlib Package of Python for Geospatial Data Analysis in Marine Geology, *International Journal of Environment and Geoinformatics*, 6(3), 225-237. doi.10.30897/ijegeo.567343.

Lin, J., Stein, R. S. (2004). Stress triggering in thrust and subduction earthquakes and stress interaction between the southern San Andreas and nearby thrust and strike-slip faults. *Journal of Geophysical Research: Solid Earth*, *109*(B2). doi.org/10.1029/2003JB002607

Mallman, E. P., Parsons, T. (2008). A global search for stress shadows. *Journal of Geophysical Research*, *113*(B12), B12304. doi.org/10.1029/2007JB005336

McCloskey, J., Nalbant, S. S., Steacy, S. (2005). Earthquake risk from co-seismic stress. *Nature*, *434*(7031), 291–291. doi.org/10.1038/434291a

McCloskey, J., Nalbant, S. S., Steacy, S., Nostro, C., Scotti, O., Baumont, D. (2003). Structural constraints on the spatial distribution of aftershocks. *Geophysical Research Letters*, *30*(12). doi.org/10.1029/2003GL017225

Nalbant, S. S., Hubert, A., King, G. C. P. (1998). Stress coupling between earthquakes in northwest Turkey and the north Aegean Sea. *Journal of Geophysical Research: Solid Earth*, *103*(B10), 24469–24486. doi.org/10.1029/98JB01491

Nostro, C., Piersanti, A., Cocco, M. (2001). Normal fault interaction caused by co-seismic and postseismic stress changes. *Journal of Geophysical Research: Solid Earth*, *106*(B9), 19391–19410. doi.org/10.1029/2001JB000426

Okada, Y. (1992). Internal deformation due to shear and tensile faults in a half-space. *Bulletin of the Seismological Society of America*, *82*(2), 1018–1040.

Omori, F. (1902). Note on the after-shocks of the Mino-Owari earthquakeof Oct. 28th, 1891. Publications of the Earthquake Investigation Committee in foreign languages.

Parsons, T. (2002a). Post-1906 stress recovery of the San Andreas fault system calculated from three-dimensional finite element analysis. *Journal of Geophysical Research*, *107*(B8), 2162. doi.org/10.1029/2001JB001051

Parsons, T. (2002b). Global Omori law decay of triggered earthquakes: Large aftershocks outside the classical aftershock zone. *Journal of Geophysical Research: Solid Earth*, *107*(B9), ESE 9-1. doi.org /10.1029/2001JB000646

Parsons, T., Stein, R. S., Simpson, R. W., Reasenberg, P. A. (1999). Stress sensitivity of fault seismicity: A comparison between limited-offset oblique and major strike-slip faults. *Journal of Geophysical Research: Solid Earth*, *104*(B9), 20183–20202. doi.org/10.1029/1999JB900056

Pollitz, F. F. (1997). Gravitational viscoelastic postseismic relaxation on a layered spherical Earth. *Journal of Geophysical Research: Solid Earth*, *102*(B8), 17921–17941.doi.org/10.1029/97JB01277

Pollitz, F. F. (2003). Transient rheology of the uppermost mantle beneath the Mojave Desert, California. *Earth and Planetary Science Letters*, *215*(1–2), 89–104. doi.org/10.1016/S0012-821X(03)00432-1

Scholz, C. H. (2019). *The Mechanics of Earthquakes and Faulting*. Cambridge University Press. doi.org/ 10.1017/9781316681473

Steacy, S. (2005). Introduction to special section: Stress transfer, earthquake triggering, and time-dependent seismic hazard. *Journal of Geophysical Research*, *110*(B5), B05S01. doi.org/10.1029/2005JB003692

Stein, R. S. (2003). Earthquake Conversations. *Scientific American*, *288*(1), 72–79. doi.org/ 10.1038/scientificamerican0103-72

Stein, R. S., Barka, A. A., Dieterich, J. H. (1997). Progressive failure on the North Anatolian fault since 1939 by earthquake stress triggering. *Geophysical Journal International*, *128*(3), 594–604. doi.org/10.1111/j.1365-246X.1997.tb05321.x

Sunbul, F., Nalbant, S. S., Simão, N. M., Steacy, S. (2016). Investigating viscoelastic postseismic deformation due to large earthquakes in East Anatolia, Turkey. *Journal of Geodynamics*, *94–95*, 50–58. doi.org/10.1016/j.jog.2016.01.002

Taylor, M. A. J., Dmowska, R., Rice, J. R. (1998). Upper plate stressing and seismicity in the subduction earthquake cycle. *Journal of Geophysical Research: Solid Earth*, *103*(B10), 24523–24542. doi.org/10.1029/98JB00755

Taylor, Mark A. J., Zheng, G., Rice, J. R., Stuart, W. D., Dmowska, R. (1996). Cyclic stressing and seismicity at strongly coupled subduction zones. *Journal of Geophysical Research: Solid Earth*, *101*(B4), 8363–8381. doi.org/10.1029/95JB03561

Toda, S., Stein, R. S., Beroza, G. C., Marsan, D. (2012). Aftershocks halted by static stress shadows. *Nature Geoscience*, *5*(6), 410–413. doi.org/10.1038/ngeo1465

Utsu, T. (1962). On the nature of three Alaskan aftershock sequences of 1957 and 1958. *Bulletin of the Seismological Society of America*, *52*(2), 279–297.

Vergnolle, M., Pollitz, F., Calais, E. (2003). Constraints on the viscosity of the continental crust and mantle from GPS measurements and postseismic deformation models in western Mongolia. *Journal of Geophysical Research: Solid Earth*, *108*(B10). doi.org/10.1029/2002JB002374

Wells, D. L., Coppersmith, K. J. (1994). New empirical relationships among magnitude, rupture length, rupture width, rupture area, and surface displacement. *Bulletin of the Seismological Society of America*, *84*(4), 974–1002.

Wright, T. J., Elliott, J. R., Wang, H., Ryder, I. (2013). Earthquake cycle deformation and the Moho: Implications for the rheology of continental lithosphere. *Tectonophysics*, *609*, 504–523. doi.org/10.1016/j.tecto.2013.07.029

APPENDICES.

Table A1. The 109 M≥7.0 Earthquakes and their analysis, used in the study.

NO	Earthquake	Mech	date	M	Lat	Long	strk	dip	rake	Number of events	CO increase	CO decrease	CO+VE increase	CO+VE decrease
1	South of Fiji Isl	S	1990	7.5	-22.1	175.35	228	68	4	13	5	4	5	6
2	Vanuatu Isl	T	1990	7.1	-18.4	168.04	350	28	104	120	6	4	9	4
3	Costa Rica	T	1990	7	9.95	-84.58	303	11	104	42	5	2	5	2
4	Mariana Isl	N	1990	7.5	15.57	148.08	185	31	-108	22	3	8	5	8
5	Minahassa Peninsula	T	1990	7.4	1.31	123.35	112	31	122	108	27	15	31	17
6	Sudan	S	1990	7.2	5.32	32.29	224	67	176	6	0	4	0	4
7	Sudan		1990	7	5.7	31.67	232	43	-131					
8	Panay, Philiphines	O	1990	7	11.7	121.86	224	78	-169	24	0	1	1	1
9	Western Iran	O	1990	7.7	36.95	49.52	200	59	160	8	4	2	4	3
10	Luzon, Philiphine Isl.	S	1990	7.8	15.97	121.23	243	86	178	40	12	15	13	16
11	Komandorsky Isl	O	1990	7	53.77	169.41	308	23	159	13	2	1	2	1
12	Burma	S	1991	7.1	23.61	96.18	2	68	166	16	0	1	1	1
13	Costa Rica	T	1991	7.5	10.1	-82.77	103	25	58	22	9	6	10	5
14	Western Caucasus	T	1991	7	42.6	43.61	288	39	106	8	2	2	2	4
15	Minahassa Peninsula	T	1991	7.1	1.04	123.23	109	7	102	86	10	23	24	25
16	Off N. California C	S	1991	7.1	41.71	-125.6	314	62	176	24	1	4	2	5
17	Solomon Isl	T	1991	7.1	-9.17	158.36	300	29	51	49	4	5	4	5
18	Northern India	T	1991	7.1	30.22	78.24	317	14	115	1	0	0	0	0
19	Near W C Colombia	T	1991	7	4.8	-77.18	13	13	95	21	0	1	1	2
20	Kuril Isl	T	1991	7.4	45.58	151.55	226	16	99	112	30	10	40	9
21	South Sandwich Isl	N	1991	7.1	-55.9	-24.48	322	31	-90	34	6	1	7	1
22	Northern California	T	1992	7.1	40.25	-124.3	331	9	68	15	4	2	12	3
23	East Papua New Guinea	T	1992	7.1	-6.35	147.59	282	34	88	120	24	18	35	22
24	Mindanao, Philiphines	T	1992	7.1	7.27	126.96	173	29	53	116	19	9	22	9
25	Mindanao, Philiphines		1992	7.5	7.33	127.18	176	25	67					
26	Cuba Reg	T	1992	7	19.84	-77.7	248	43	-1	1	0	0	0	0
27	Santa Cruz	N	1992	7	-11.2	165.06	168	35	-84	155	20	20	21	24
28	southern California	S	1992	7.5	34.65	-116.7	341	70	-172	14	5	4	4	7
29	Kirghiz	T	1992	7.4	42.19	73.32	250	31	74	5	2	2	2	2
30	N of Ascension Isl	S	1992	7	-0.71	-13.54	256	81	-179	11	3	1	3	1
31	N C of Nicaragua	T	1992	7.2	11.2	-87.81	303	12	91	87	15	1	14	5
32	North Colombia	T	1992	7.3	7.27	-76.34	270	45	167	16	1	4	1	4
33	Flores Isl	T	1992	7.5	-8.34	122.49	80	40	95	27	7	4	11	4
34	Santa cruz	T	1993	7.2	-10.7	164.02	252	55	7	102	13	9	18	8
35	Near E C of Kamch	T	1993	7.3	51.36	158.75	207	29	79	73	28	5	36	2
36	Hokkaido, Japan	T	1993	7.6	42.71	139.28	179	55	90	8	1	3	2	4
37	S of Maraiana Isl	T	1993	8.1	13.06	145.31	312	18	147	82	34	25	36	28
38	off W C of S Isl	T	1993	7.1	-45	166.73	46	29	127	8	1	4	1	4
39	Near C of Chiapas	T	1993	7.3	14.41	-92.99	289	24	76	84	20	11	22	14
40	East Papua New Guinea	T	1993	7.1	-6.04	146.11	310	8	110	94	5	4	6	4
41	East Papua New Guinea	T	1993	7.1	-5.87	145.99	291	20	79	84	2	0	4	1
42	Near E C of Kamch	T	1993	7.1	52	159.27	206	31	83	89	24	8	27	8
43	Halmahera	S	1994	7.2	1.2	127.8	83	66	174	186	3	11	5	11
44	Vanuatu Isl	T	1994	7.2	-20.5	169.04	335	40	90	149	19	5	20	8
45	S Sumatera	S	1994	7	-5.15	104.27	315	71	176	92	0	0	0	0
46	S of Java	T	1994	7.2	-11	113.04	278	7	89	31	14	0	11	2
47	S Isl, New Zealand	T	1994	7.1	-42.9	171.47	68	63	150	8	1	1	1	1

48	Vanuatu Isl	O	1994	7.4	-16.5	167.35	272	42	2	165	12	5	13	5
49	Off C of Northern CA	S	1994	7	40.59	-125.8	274	65	176	17	5	6	6	7
50	Kuril Isl	T	1994	7	43.87	147.96	227	19	104	143	46	10	56	13
51	Mindoro, Philippine Isl	S	1994	7.1	13.44	121.32	339	70	-178	44	5	2	5	3
52	Off east C Honshu	T	1994	7.5	40.56	142.99	179	12	67	159	54	11	57	15
53	West Irian Reg	S	1995	7.1	-4.18	135.1	257	80	-4	65	5	18	6	17
54	Samar, Philippine Is	T	1995	7	12.17	126.03	145	26	43	81	23	8	21	9
55	Samar, Philippine Is	T	1995	7.3	12.27	125.69	153	22	61					
56	Samar, Philippine Is	T	1995	7	12.67	125.3	145	16	65	66	14	7	14	11
57	Loyalty Isl	N	1995	7.7	-23.1	170	280	35	-99	154	54	64	52	59
58	Sakhalin Isl	S	1995	7.6	53.03	142.65	287	79	8	7	3	4	3	4
59	Kermadec Isl	T	1995	7.2	-29.1	-177.2	197	28	95	164	13	3	18	4
60	Burma China Border	S	1995	7.2	21.89	99.22	60	85	1	0	0	0	0	0
61	Near C of Nort. Chile	T	1995	7.3	-24.2	-70.74	354	22	87	49	7	5	10	6
62	Solomon Isl.	T	1995	7.8	-5.51	153.64	136	42	87	354	126	68	139	81
63	Solomon Isl.		1995	7.2	-6.08	154.19	133	45	91					
64	Near C of Guerrero	T	1995	7.2	16.73	-98.54	289	15	85	42	14	0	17	0
65	Peru-Ecuador Border	T	1995	7	-2.55	-77.53	234	39	120	26	3	1	3	1
66	Near C of Jalisco	T	1995	7.3	19.34	-104.8	302	9	92	30	5	0	7	0
67	Arab Rep of Egypt	O	1995	7.3	29.07	34.73	196	59	-15	3	1	2	1	2
68	Minahassa Peninsula	O	1996	7.7	0.74	119.93	36	6	54	56	22	12	19	15
69	Kuril Isl	T	1996	7	45.29	150.45	235	28	113	76	10	4	14	4
70	West Irian Reg	T	1996	8.1	-0.67	136.62	103	11	69	43	18	11	22	11
71	Solomon Isl	T	1996	7.5	-6.65	155.07	138	45	99	235	43	19	51	18
72	Andrean of Isl	T	1996	7.6	51.1	-177.4	248	17	84	100	67	16	66	16
73	Andrean of Isl		1996	7.1	51.38	-176.5	258	25	105					
74	Samar, Philippine Is	T	1996	7	12.74	125.41	144	23	60	52	11	7	11	7
75	Solomon Isl	T	1996	7.1	-10.8	161.46	139	50	139	86	14	14	18	12
76	Easter Isl	T	1996	7	-22.3	-113.3	93	45	69	136	1	3	2	3
77	Near C of Peru	T	1996	7.3	-15	-75.37	312	33	55	49	10	2	14	3
78	Eastern Kashmir	O	1996	7.1	35.45	77.86	180	71	170	5	0	1	1	1
79	Pakistan	T	1997	7.3	29.74	68.13	298	15	122	21	5	3	10	6
80	Santa Cruz	T	1997	7.9	-13.2	166.2	301	39	40	201	33	42	57	50
81	Iran	S	1997	7.3	33.58	60.02	248	83	0	7	1	2	1	3
82	Kermadec Isl	T	1997	7	-28.8	-177	195	29	90	222	24	1	35	1
83	Tibet	O	1997	7.9	35.33	86.96	79	69	2	3	1	2	1	2
84	Near C of Kamch	T	1997	7.6	54.31	161.91	202	23	74	70	27	9	30	11
85	Balleny Isl	N	1998	8	-63	148.64	189	73	174	6	0	5	0	5
86	Southeast of Taiwan	S	1998	7.3	22.37	125.53	139	82	1	16	1	5	1	5
87	Near c of Papua N G	T	1998	7.1	-2.5	142.07	146	19	127	82	10	6	11	7
88	Near C of Ecuador	T	1998	7.1	-0.57	-80.48	27	15	124	23	7	0	8	0
89	Banda Sea	T	1998	7	-6.94	128.95	289	37	111	161	4	6	10	6
90	Ceram Sea	S	1998	7.7	-2.03	125	92	63	-28	72	12	7	18	8
91	New Britain Reg.	T	1999	7	-4.99	152.76	262	28	96	438	55	20	55	25
92	Turkey	S	1999	7.8	41.01	29.97	182	74	3	10	3	7	3	7
93	Taiwan	T	1999	7.7	24.15	120.8	37	25	96	126	22	63	38	55
94	Oaxaca, Mexico	N	1999	7.5	16.2	-96.96	102	42	-103	38	5	7	5	14
95	Southern California	S	1999	7.4	34.71	-116.3	336	80	174	11	3	1	2	2
96	Turkey	S	1999	7.5	40.93	31.25	268	54	-167	6	0	1	0	1
97	New Britain Reg.	T	1999	7	-6.27	149.03	279	35	103	201	22	5	28	5
98	New Britain Reg.	T	1999	7	-6.49	148.98	275	25	100					
99	Vanuatu Isl	T	1999	7.3	-16.1	168.31	174	30	67	243	83	22	107	34
100	Luzon, Philiphine Isl.	T	1999	7.1	15.87	119.64	112	13	169	42	2	1	3	1
101	Vanuatu Isl	S	2000	7.1	-19.6	174.17	315	74	169	32	0	0	0	0

102	Sulawesi	T	2000	7.5	-1.29	123.59	225	64	172	104	9	10	10	12
103	Southern Sumatera	T	2000	8	-4.73	101.94	92	55	152	213	84	69	92	72
104	South Indian Ocean	T	2000	7.8	-13.5	97.17	161	63	-5	4	0	2	0	2
105	Sakhalin Isl	T	2000	7.1	48.77	142.03	328	36	60	7	1	2	1	2
106	New Ireland (SEQ)	T	2000	8.2	-4.56	152.79	328	43	3	540	192	172	231	182
107	New Ireland (SEQ)		2000	7.8	-5.03	153.17	253	15	93					
108	New Britain Reg.(SEQ)	T	2000	8	-5.26	152.34	230	24	64					
109	Turkmen	T	2000	7.5	39.6	54.87	319	33	136	5	2	1	2	1